Electronic Supplementary Material (ESI) for Lab on a Chip.

NemaFlex: A microfluidics-based technology for standardized measurement of muscular strength of *C. elegans*

Mizanur Rahman,[a] Jennifer E. Hewitt,[a] Frank Van-Bussel[b], Hunter Edwards[a], Jerzy Blawzdziewicz[b], Nathaniel J. Szewczyk[c], Monica Driscoll[d] and Siva A. Vanapalli*[a]

[a] *Department of Chemical Engineering, Texas Tech University, Lubbock, TX 79409, USA. E-mail: siva.vanapalli@ttu.edu*
[b] *Department of Mechanical Engineering, Texas Tech University, Lubbock, TX 79409, USA. E-mail: jerzy.blawzdziewicz@ttu.edu*
[c]*MRC/Arthritis Research UK Centre for Musculoskeletal Ageing Research, University of Nottingham, Derby DE22 3DT, UK. E-mail: nathaniel.szewczyk@nottingham.ac.uk*
[d]*Department of Molecular Biology and Biochemistry, Rutgers University, Piscataway, NJ 08854, USA. E-mail: driscoll@dls.rutgers.edu*

Electronic Supplementary Information (ESI)

Supplementary Materials is uploaded as a separate file. List of the items are

Supplementary Note 1. Image processing for measurement of pillar displacements.

Supplementary Note 2. Validity of the force-deflection expression.

Supplementary Note 3. Design considerations for the micropillar arena.

Supplementary Note 4: Average force value does not reliably capture *C. elegans* muscle strength.

Supplementary Figure.1. Work flow of pillar tracking algorithm.

Supplementary Figure 2. Wall effects on estimating strength measures.

Supplementary Figure 3. Suitability of Timoshenko beam deflection theory to estimate pillar forces.

Supplementary Figure 4. Average force value does not reliably capture *C. elegans* muscle strength.

Supplementary Figure 5. Size distribution of synchronized (young adult) wild-type population.

Supplementary Table 1. Estimates of default pillar deflection and forces due to the nematode body size being greater than the gap between pillars.

Supplementary Table 2. Previous studies of the influence of pillar arena/geometry on *C. elegans* locomotive behavior and force generation.

Supplementary Video 1: Tracking of pillar deflections using NemaFlex software. A crawling *C. elegans* deflects pillars as it navigates through the pillar arena (confinement >1 in this example). Each deflected pillar is tracked individually during the entire period of its deflection by fitting a circle on the pillar projection. Blue circles represent the undeflected location of a pillar and the red circles represent the deformed pillars due to active pushing by the nematode. The movie plays at a speed of 10 fps.

Supplementary Video 2: Illustration of pillar deflection measurement. Post-processed and assembled movie showing high resolution fitting of pillar deflections. Momentary touching of the pillars by the worm is also picked up by the software indicating the high fidelity in tracking pillar displacements. The movie plays at a speed of 10 fps.

Supplementary Video 3: Response in applied force on pillars by a nematode in varying degree of confinement. Worm movement and interaction with pillars in (**a**) arena A1 (confinement = 0.70) and (**b**) arena A3 (confinement = 1.1, same worm). As the confinement increases from A1→A3, the worm pushes the pillars harder to make its way through, causing larger maximal forces (in this case in arena A3). The movie plays at a speed of 6 fps.

Supplementary Video 4: Changes in the size and behavior of a nematode in response to acetylcholine agonist levamisole. (**a**) A typical crawling episode of a worm in NemaFlex in absence of levamisole (confinement > 1.1). (**b**) The same worm undergoes a length contraction by approximately 11% and exhibits mostly reverse crawling under the influence of levamisole. The dosage used here is sub-lethal. The movie plays at a speed of 6 fps

NemaFlex software

The NemaFlex software package that contains the MATLAB script files, custom-written routines, spreadsheet for calculating pillar stiffness, standard operating procedure for running the codes, and sample movies are provided at this link:

https://www.dropbox.com/sh/buxcuuks33almjq/AAB5TYXEQSzdv8Za5xx8yjYka?dl=0

Supplementary Note 1: Image processing for measurement of pillar displacements

The overall procedure for tracking pillar deflections involves the following steps (**Supplementary Figure 1**): (i) standard image preprocessing. In this step, worms are isolated from the image as the foreground and pillars are retained in the background. (ii) Generation of mask. The mask is generated from foreground image and is used to mask out the untouched pillars. (iii) Object tracking for image objects (worm, pillar and other objects). (iv) Pillar array (grid) identification and grid verification. In this step, pillars are identified using circular Hough transform (CHT) and verified for their grid location. (v) Determination of pillar base location and radius when the pillar is not touched by the worm and (vi) deflection measurements with reference to the pillar base location.

(i) *Image preprocessing:* A median filter is applied to each image (main tex**t Fig. 2a)** to eliminate the outlier pixels. A standard thresholding technique (Otsu's method) is used to calculate the threshold to obtain the foreground and background images[1]. The maximum pixel value (i.e. brightest) at each pixel location across all frames provides the background image. Likewise, the minimum pixel value (i.e. darkest) at each pixel location yields the foreground image. As shown in **Fig. 2b** (main text), these operations make the worm's entire trajectory visible in the foreground image and absent from the background image. The background contains mostly pillars (see main text **Fig. 2c**) and extraneous objects not part of the worm's trajectory.

(ii) *Mask generation and identification of interacting pillars:* The standard image processing technique of background subtraction cannot be used to identify the interacting pillars because they are in the background. Moreover, many pillars are never touched by the worm in the entire movie and tracking all of them will be computationally expensive. In order to avert background subtraction and isolate only the deflected pillars, a "mask" is created, which as shown in main text **Fig. 2d** contains the worm trajectory with contiguous pillars only. This mask is generated by segmenting the foreground using the threshold and regionprops operations. As the worm trajectory is the largest object in foreground, keeping the largest object by area in the mask will retain the regions where the worm is interacting with the pillars and eliminates the untouched pillars. The circles on the mask are then filled and dilated.

(iii) *Tracking of objects:* Once the mask is generated from the entire image stack, we apply it to each of the video frames and determine contiguous objects (main text **Fig. 2f**) using regionprops function based on the nearest neighbor algorithm[2]. Taking all the contiguous objects identified, we impose area-based cutoffs to sort the worms and pillars. Typically, we find that the worms are approximately 2 orders of magnitude larger than pillars. Frame-to-frame tracking is done separately for these different objects with slightly different criteria for track persistence. Worm-objects are tracked between frames using their centroid, and the trajectory is terminated if the size changes dramatically (e.g. when a given worm encounters another worm or an air bubble). The centroids of pillar objects are identified, and tracks are created for each pillar object, which we call pillar- object-track (POT). If a pillar in a particular frame is touching a worm, then the corresponding POT will have a gap at that point. Thus, the gap information in the pillar track determines the frames when the pillar was deflected and is used for deflection measurement. The rest of the frames are used for determination of pillar base location and radius. Thus, the POTs contain only the untouched pillars. This approach reduces the computation time significantly.

(iv) *Identification of approximate pillar coordinates in the arena.* Independent of steps (ii) – (iii), in parallel, we take the background image (main text **Fig. 2c**) and analyze it to identify the approximate coordinates of each pillar. Given that experimentally, the rows of pillars are slightly misaligned with respect to the image edge, here we also calculate the rotation angle for the background image to correct this misalignment.

To identify the approximate pillar coordinates, we apply the CHT, which finds the rims of pillars in the background image[3]. We note that implementing MATLAB's *imfindcircles* does not locate all the pillar rims, because it is optimized to find filled disks. In addition, as shown in the main text **Fig. 2h**, rather than having uniform thin-rimmed annuli, the pillar rims are somewhat like the Chinese Taijitu (i.e. Yin-Yang) symbol when being pushed hard by the worm. It is found that imfindcircle often fails to locate actual pillar rims in this case.

To address this issue, we implement the CHT where it looks for as many circles as it can with a given radius (user supplied) plus or minus 10% (main text **Fig. 2e).** Our own implementation is designed to find open rings in binary images. It works most robustly when rims of the circles in the image are at most 3 pixels thick, so a prior attenuation operation (either skeletonization or outlining) is done in each phase. We note that when the CHT checks for multiple radii this is computationally equivalent to running multiple passes checking for individual radii one at a time, so radii within the range are accurate up to a given resolution, which in this case will be 1/2 pixel.

Our CHT implementation tries to find all possible rings, implying that some of them may not be actually rims of pillars. To eliminate the false pillar rims, we generate a grid based on user-defined spacing (see main text **Fig. 2h**). To align the grid onto the pillar-containing image, we check for rotation with respect to the viewpoint by taking the median of the angles between nearest neighbors. After rotation, the frame is translated by taking the medians of the x and y components of the difference between the generated grid points and their nearest found

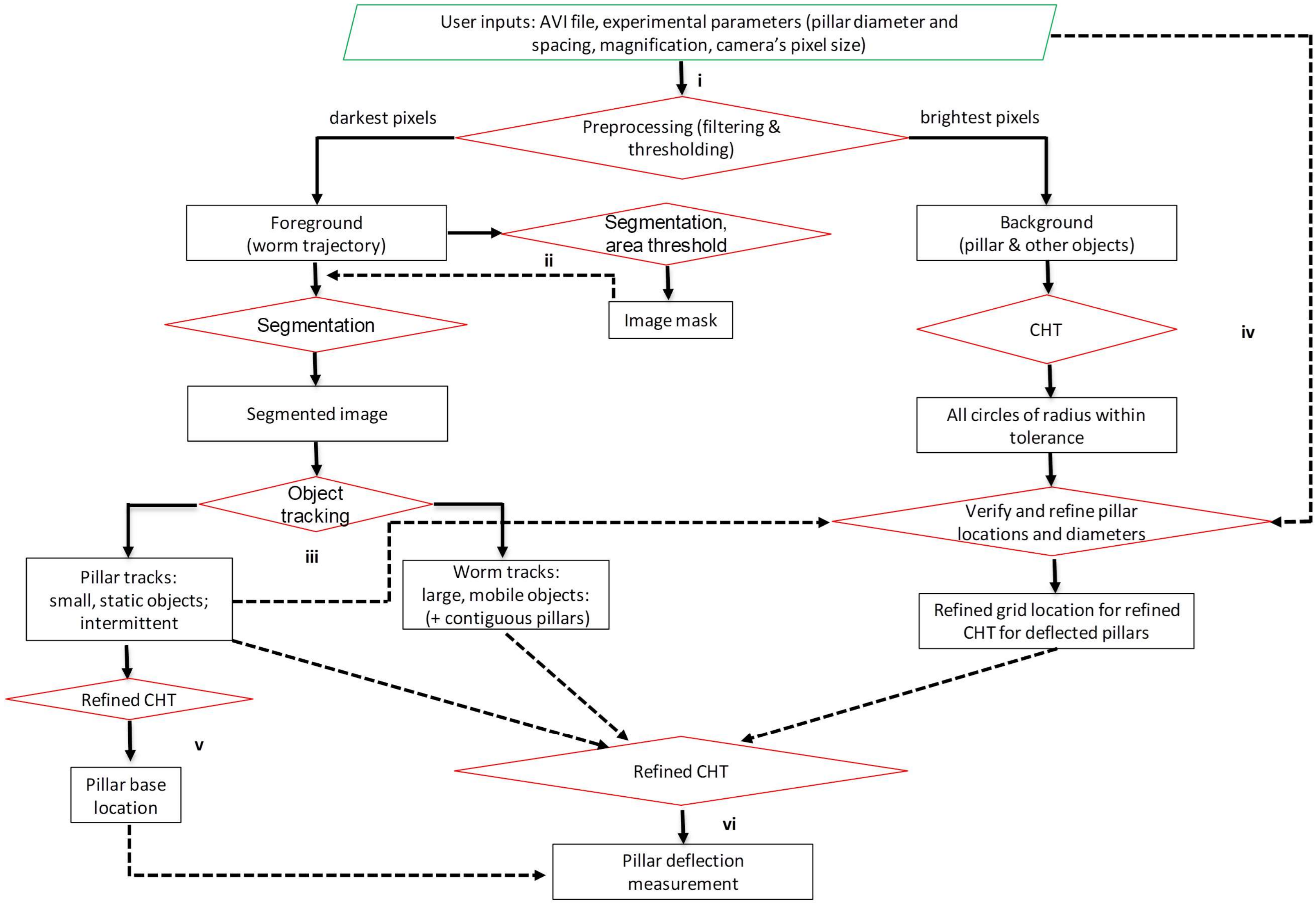

Supplementary Figure 1. Work flow of pillar tracking algorithm. The listed steps (i) – (vi) are described in Supplementary Note 1.

140

circles. Finally, we cross-reference the intersection points of the aligned grid with the centers of all possible rings and determine the rings that truly correspond with the pillars.

(v) *Determination of pillar base locations:* The pillar base locations are needed as a reference point to determine deflections. We do this by taking POTs from step (iii), which contain the undeflected pillars. These undeflected pillars are verified by checking their centroids against the grid locations (main text **Fig. 2g**) as well as checking for general shape conformance to a circle. Since the POTs contain several instances of the same undeflected pillar, we only take a subset of frames that yield the best shape conformance. The center and pillar radius values are evaluated for pillars that satisfy the grid positions and the best shape conformance. This refining is done using the CHT, this time in single-circle multi-radius mode on a small subframe containing the pillar-object.

We note that when we apply the CHT, the pillar rims are reduced to 2-3 pixels lining the interior of the rim (see main text **Fig. 2i**), since of all the alternatives available this corresponds most closely to the actual pillar extents. If we do not perform this attenuation operation, the radius value is too large since shadowing is more extensive outside than inside the pillar.

In general, we find that our videos contain at least one image where the undeflected states of an interacting pillar is captured, allowing us to accurately determine the pillar base location (as described above). In some rare instances, we may not have the untouched location of an interacting pillar, for example, if the worm touches the pillar in question during every frame of the movie. Although, it is possible to approximate the base location for such pillars using the base location of neighbouring pillar and array geometry, the deflections of these pillars are not considered in the analysis.

(vi) *Pillar deflection measurements:* To measure the deflections, the worm-objects that have contiguous pillars are taken (from the images that correspond to the gaps in POTs), and a single-circle, single-radius CHT is applied in a box with sides approximately twice the base diameter centered on the base location. We note that the attenuation operation, similar to the detection of untouched pillar base location, is also applied here.

In some instances, we do observe large deflections of the pillars, in which case the interior region of the pillar is more of an ellipse rather than a circle. Even in this case, the CHT works (main text **Fig 2j**) because the exterior perimeter in the direction of deflection will give a fairly trustworthy view of the actual pillar circumference since the shadowing is all on the inside of the pillar image (caused by light scattering due to the rounded sides of the pillar). In the other direction, the shadowing is blocked by the worm's body, but the pillar itself is hard enough to press into the worm without being noticeably deformed. Due to tilt the actual shape is an ellipse, but the eccentricity is low enough that the CHT still finds a circle using the base radius.

Interaction of animals with sidewalls of pillar chamber and its effect on strength (f_{95}): We found that animals sometime prefer to interact with the side walls of the pillar arena. We observed that worms either (i) crawl along the wall and come back to the main arena in a continuous stroke (**Supplementary Figure 2a**), or (ii) move back and forth along the wall and spends longer duration along the wall (**Supplementary Figure 2b**), or (iii) try to make turns between the narrow space of the wall and the very first pillar from the wall (**Supplementary Figure 2c**).In case (i), f_{95} calculated for the frames where the worm body is touching the wall was found to be less than the f_{95} for the frames when the worm was not touching the wall (**Supplementary Figure 2d**). In case (ii), f_{95} could not be calculated as there was no frame available in which the worm did not touch pillars precluding us from determining the location of the pillar base. In case (iii), animal struggles to carry the whole body through the narrow space and the vector sum of the pillar forces is far from zero (> 10% of the total force generated by the worm) indicating animals exert significant forces on the walls. Thus, in evaluating f_{95} we censored those frames where worms were found to be interacting with the walls. We typically considered those pillar deflections where the animals were crawling approximately 300 - 500 µm away from the side walls.

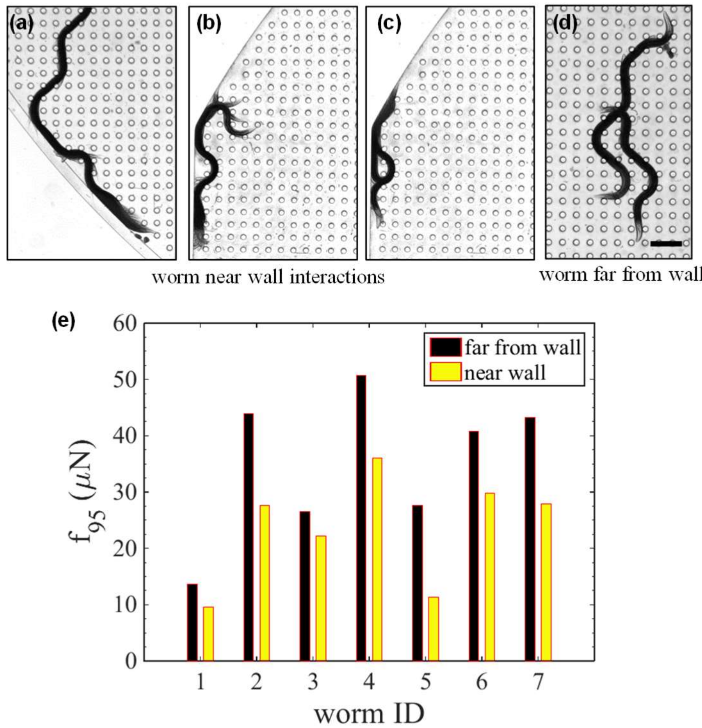

Supplementary Figure 2. Wall effects on estimating strength measures. *C. elegans* exhibit three types of interaction with the side wall of NemaFlex. Animal (a) crawl along the wall and come back to main arena in a continuous stroke (88 frames), (b) confused and move back and forth along the wall (64 frames), (c) try to make turns between the narrow space of the wall and the very first row of pillar from the wall (50 frames), and (d) worm crawling far from the wall (40 frames). Images are shown by overlaying min pixel intensity across all frame used. Scale bar 200 μm. (e)The maximum exertable force (f_{95}) calculated when the worms are far from the wall is consistently higher than the case when the worms interact with the walls.

Supplementary Note 2: Validity of the force-deflection expression

In the NemaFlex device, the forces exerted by *C. elegans* on the pillars are estimated using the elastic Timoshenko beam deflection model[4],

$$F = k\Delta = \frac{\Delta}{\left(\frac{l^3}{3EI} + \frac{a^2(1+\gamma)l}{4EI} + \frac{l^2(h-l)}{2EI}\right)} \qquad (1)$$

where *Δ* is the deflection and *k* is the stiffness of the micropillar. The definitions of parameters in *k* are described in the main text.

The accuracy of the force calculation depends on the following factors: (i) aspect ratio of the pillar, *i.e.* ratio of height to diameter, (ii) magnitude of pillar deflection, (iii) constitutive law for the material used to fabricate pillars which is influenced by loading rate, and (iv) location where the force is applied on the pillar. Below we discuss the impact of each of these factors on our force analysis.

(i) *Pillar aspect ratio*. For slender micropillars of aspect ratio > 10, the Euler beam theory can be used to calculate the forces. However, for pillars of low aspect ratio, the bending due to shear needs to be considered as well. The pillars in the NemaFlex device that have been used predominantly in the study have a diameter of a = 38.3 ± 0.4 µm and h = 71.8 ±2.9 µm, giving an aspect ratio of 1.9 ± 0.08. Due to this low aspect ratio we have used the Timoshenko beam theory to calculate the forces from deflected pillars. In a recent study, Du *et al.* have shown that for pillars of aspect ratio 1.6, Euler beam theory overestimates forces by as much as 29.3 %, whereas Timoshenko beam theory predictions are within 5% of the experimental data[5].

(ii) *Magnitude of pillar deflection*. The extent of pillar displacements in our study typically vary from, Δ/h = 2.5-19.3%. Xiang and LaVan and Lin *et al.* have investigated behavior of low aspect ratio PDMS pillars across a wide range of deflections, Δ/h = 0 – 70% [6, 7]. They showed that the predictions from the Timoshenko model are within 10% when $\Delta/h \leq 20\%$. Thus, using Eqn. (1) does not contribute large errors, even though the pillars in our study are of low aspect ratio and undergo reasonably large deflections.

We also tested the validity of the Timoshenko beam relation to the experimental data of PDMS pillar displacement reported by Khare *et al.*, in which they focused on measuring forces generated by *C. elegans*[8]. The authors directly obtained the force-deflection relation by measuring micropillar displacement as a function of applied force by using a FemtoTools force sensor. The PDMS pillars were of aspect ratio 3 and the deflection range was Δ/h = 0 – 33%. As shown in **Supplementary Figure 3a**, their data fits well to Eqn. (1).

(iii) *Constitutive law*. In this study, we assume that the PDMS pillars are elastic, i.e. the rate at which the nematode pushes the pillars does not influence our force estimates. However, depending on the loading rate, PDMS can be a viscoelastic material[9]. In the study by Lin *et al.,* they showed that when the loading rate is varied from 1.33 – 133 µm/sec, both the elastic and viscoelastic Timoshenko beam theory agree within a margin of 5% error for a deflection range of Δ/h = 0-10%[5]. In our experiments, *C. elegans* push the pillars at a very small loading rate of 0.2 – 2.26 µm/sec, and the corresponding deflections are less than 20 %. Therefore, the elastic Timoshenko beam model suffices for our force analysis[5, 10].

The PDMS modulus value used in this study is E = 2.6 MPa, which was obtained from literature[9, 11, 12]. The procedure used in our work to fabricate the PDMS pillars is very similar to that used in these prior studies suggesting this value is an appropriate choice. Any error in estimating E does not alter the trends reported in this study.

(iv) *Point of force application*. An important consideration in the force calculation is the choice of where exactly on the pillar the worm is applying its load, denoted by the parameter l in Eqn.

(1). Assuming the applied force is a point load, one obvious choice is that the load is being applied from the center of the worm body width as shown in **Supplementary Figure 3b** as option I. The second choice is that the load is being exerted at the center of the projected area that the worm body presses against the pillar, shown as option II in **Supplementary Figure 3b**. For the two choices, the estimated forces vary by 17% for L4 and 26% for the fully developed worms.

In this study, we used option II since experimentally we observe that force applied on the pillar by the worm causes local deformation in the worm body, and the contact force appears to be distributed across the worm cuticle. Moreover, when using option I, we find that in some cases $l > h$, making it unphysical in the sense that the location where the load is being applied is not actually on the pillar.

In summary, considering all the factors that might influence the accuracy of force calculation, Eqn. (1) is a reasonable choice for determining forces from the pillar deflections for the micropillar geometry used in our study. Any inaccuracies will propagate the error, however, the trends we report will remain unchanged since the same analysis procedure was used in the entire study.

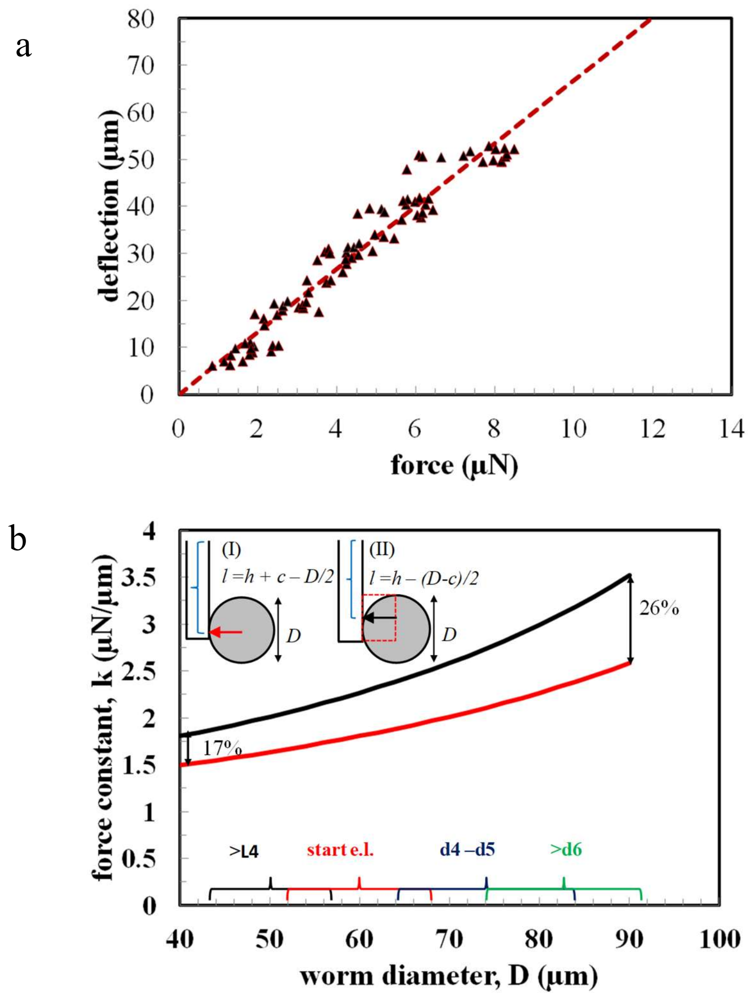

Supplementary Figure 3. Suitability of Timoshenko beam deflection theory to estimate pillar forces. (a)Timoshenko beam deflection theory estimates reaction forces from a PDMS micropillar with good agreement for deflections created artificially with a FemtoTools© force sensor. Each scatter symbol represents a deflection caused by a FemtoTools© force sensor using known force. Data is from the literature[8]. The line represents the elastic Timoshenko model (Equation 1). Pillar dimensions are *a* =50±0.58 µm; *h*=153±5.24 µm; *s* =70±0.58 µm and point of the load is 25 µm above from the tip of the pillar. (b) Timoshenko beam deflection theory is sensitive to the assumption of point where the load is applied. Solid lines in red and black represent the force for unit deflection calculated using the two different options illustrated in the inset. In this study option II has been used. The worm diameter considered here ranges from L4 to fully developed worms (e.l. indicates egg laying.)

Supplementary Note 3: Design considerations for the micropillar arena

The main considerations for designing the micropillar arena are to (i) match closely the crawling gait (wavelength and amplitude) of *C. elegans* on agar, (ii) maximize the number of pillars deflected by the worm body, and (iii) accommodate the limits imposed by the elastic Timoshenko beam deflection theory.

Our worms of interest for muscle strength measurement were L4 (46-50 hrs, D = 50-55 µm,) to young adult (60-65 hrs old, D = 58-67 µm). We ensured that the diameter of the pillars was not too small such that significant deflections occurred violating the limits of Timoshenko beam deflection theory. Likewise, designing too large a diameter of pillars makes the pillars so stiff that the deflections are rather small and below the camera resolution. Pillars of diameter a = 50 µm were used in previous force measurement assays and the maximum reported force was 35 µN[11, 13]. The deflection equivalent to this amount of force is (for a 50 µm diameter pillar) within the limit of Timoshenko beam deflection model as well as the camera resolution. As a result, in this study, we explored pillars with $a \approx 40 – 60$ µm.

The edge-to-edge spacing between pillars *(s)* was designed such that the nematodes could crawl freely without getting stuck. To quantify the degree of free space available for the nematode to crawl, we define a confinement parameter D/s. Smooth crawling for day 3 young adult *C. elegans* was reported by Albrecht *et al.* in an arena containing non-deformable pillars with a = 200 µm and a confinement D/s = 0.58[14]. Initial trials showed that a device with this level of confinement produced forces that are too small, and the animals are not challenged enough to push the pillars.

Using the above heuristics, we tested a microfluidic device that contained a composite arena with three levels of confinement due to the distinct pillar regions A1, A2, and A3. The pillar dimensions and confinements for each of the pillar regions are listed in **Supplementary Table 1**. The crawling amplitude A and wavelength λ of young adults crawling on agar have been reported to be 100 ± 10 and 830 ± 20 µm respectively[15]. The data in **Supplementary Table 1** shows that in the composite arena the amplitude is similar to that of agar, but the wavelength is reduced significantly. Yet, we observe that the animals are able to crawl without getting physically immobilized. Similar observations were made by Albrecht *et al.* who reported crawling wavelength of 520 µm and amplitude 150 µm for an adult worm in their non-deformable micropillar arena[14]. Thus, the nematodes are able to crawl without getting stuck even in arena A3, which has the strongest confinement of 1.16. However, the crawling velocity is reduced in arena A3 suggesting that this micropillar geometry provides a stronger physical challenge to the worm compared to the A2 and A1 arenas.

Supplementary Note 4: Average force value does not reliably capture *C. elegans* muscle strength.

Past studies have used an average force value as the metric to report the voluntary forces that *C. elegans* exerted on the interacting pillars. Here f_{avg} is defined as the average force registered per pillar, which is then averaged over all frames[8]. To check the reliability of f_{avg} in scoring *C. elegans* muscle strength, we used the same force data (for both WT and *unc-112*) that has been used in **main text, Fig. 8**. We found that the slope is consistently lower than unity for wild type between the arenas for wild type as shown in **Supplementary Fig. 4a,b.** Coefficient of determination (r^2 value) is negative for WT in the region A1 and A3. Also, r^2-value is negative for *unc-112* in both A1 and A2 when compared to A3 as shown in the table of **Supplementary Fig. 4** indicating that the f_{avg} in different arenas do not correlate well and therefore are inconsistent metrics of muscle strength**.**

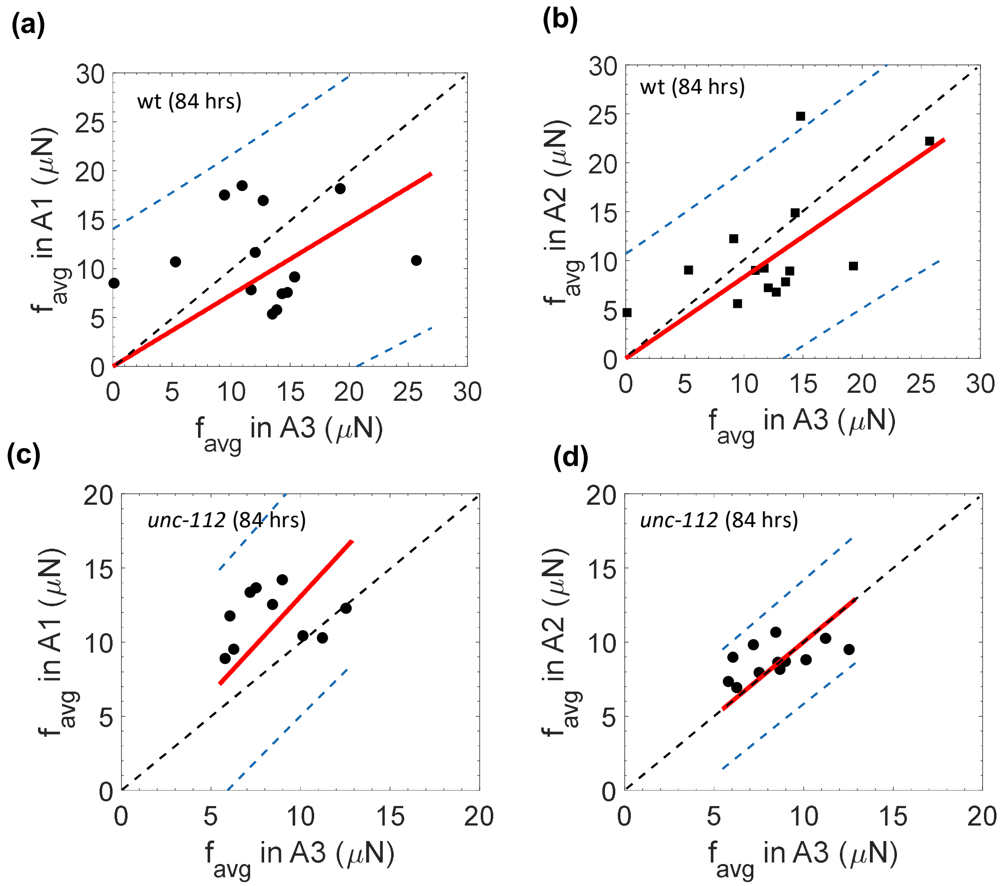

y =mx			
Genotype	Comparison	Slope, m mean ± s.e	R^2
WT	A1 vs A3	0.73 ± 0.14	-9.1
	A2 vs A3	0.83 ± 0.11	0.3
unc-112	A1 vs A3	1.3 ± 0.14	-2.35
	A2 vs A3	1.0 ± 0.07	-1.55

Supplementary Figure 4. Average force value is not a reliable measure of *C. elegans* muscle strength in pillar arena. A comparison between average exertable force measured for WT individuals in (a) section A1 and section A3, n= 14 and (b) in section A2 and section A3, n= 14. Similar comparison is shown for *unc-112* animals (n = 13 animals) in (c) and (d). The red line is the best-fit curve to the data, and the dashed black represents (slope of 1 and zero intercept). The blue lines demarcate the 95% confidence interval region. Bottom table shows the slope and coefficient of determination of the fit between pair of sections.

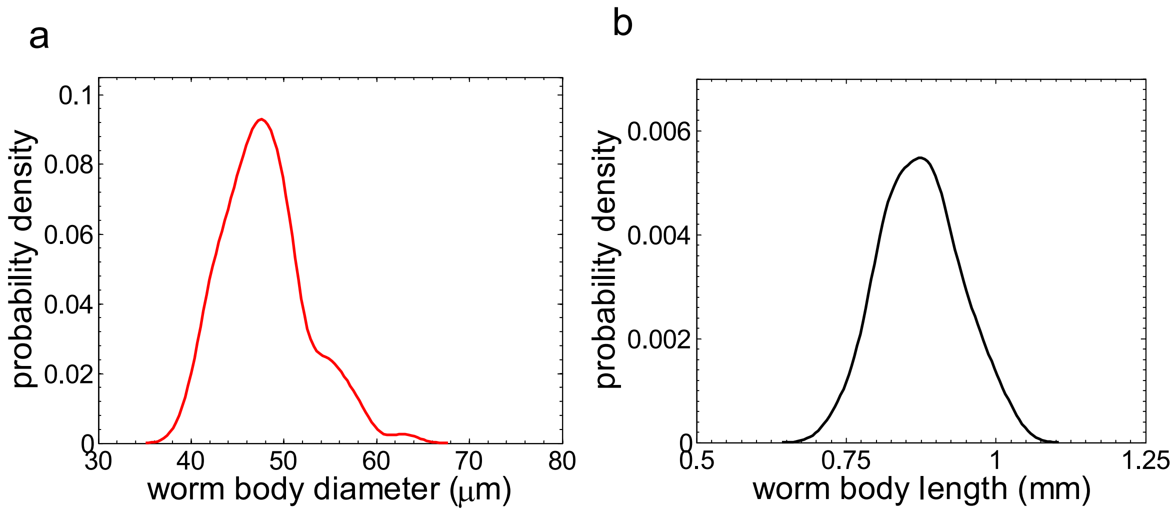

Supplementary Figure 5. Size distribution of synchronized (young adult) wild-type population. Worms grow with a wide range of sizes during the same developmental period. (a) Distribution of the worm body diameter of age-synchronized young adults, n= 98. (b) Distribution of worm lengths from the same population as in (a). Worms were grown on agar plate at 20°C with sufficient food.

Supplementary Table 1. Estimates of default pillar deflection and forces due to the nematode body size being greater than the gap between pillars.

Arena type	Pillar diameter, a µm	Worm diameter, D µm	Pillar spacing, s µm	Confinement, D/s	Default deflection, Δ =(s -D)/2 µm	Force equivlent to the deflection, F µN
Composite (A3)	44.1	64.0		1.15	4.1	11.5
	44.1	60.0	55.9	1.07	2.1	5.5
	44.1	56.0		1.00	0.1	0.1
NemaFlex	38.3	70.0		1.13	4.2	8.2
	38.3	66.0	61.7	1.07	2.2	4.0
	38.3	62.0		1.00	0.1	0.3

Supplementary Table 2. Summary of prior works that investigated the influence of pillar arena geometry on *C. elegans* locomotive behavior and force generation. The full citation of the references mentioned here are provided in the main text.

<table>
<tr><th>Focus area</th><th>Pillar diameter a , µm</th><th>Pillar spacing (center -center) So , µm</th><th>Gap between pillars $S=(So-a)$, µm</th><th>worm diameter D , µm</th><th>Pillar arrangement</th><th>Worm confinement (D/S)</th><th>Frequency f , Hz</th><th>Amplitude A , µm</th><th>Wavelength λ , µm</th><th>speed v , mm/s</th><th>reference</th></tr>
<tr><td rowspan="6">Locomotion/ behavior</td><td>100</td><td>160-200</td><td>60</td><td rowspan="3">80</td><td rowspan="3">Hexagonal</td><td>1.33</td><td rowspan="3">-</td><td rowspan="3">-</td><td rowspan="3">400 – 600</td><td rowspan="3">0.14 ± 0.017</td><td rowspan="3">ref.35</td></tr>
<tr><td>200</td><td>260-300</td><td>80</td><td>1</td></tr>
<tr><td>500</td><td>560-600</td><td>100</td><td>0.8</td></tr>
<tr><td>300</td><td>350-550</td><td>50 - 250</td><td>60</td><td>Square</td><td>0.24 - 1.2</td><td>1.92 ± 0.08</td><td>-</td><td>650 ± 40</td><td>> 1.3</td><td>ref.36</td></tr>
<tr><td>200</td><td>300</td><td>100</td><td>60</td><td>Hexagonal</td><td>0.6</td><td>-</td><td>150.00</td><td>500.00</td><td>0.20</td><td>ref.37</td></tr>
<tr><td>350</td><td>430-700</td><td>80 - 350</td><td>60</td><td>Square</td><td>0.75 - 0.17</td><td>1.5 - 2</td><td>-</td><td>-</td><td>0.1 -0.35</td><td>ref.38</td></tr>
<tr><td rowspan="5">Force</td><td>40</td><td>100</td><td>60</td><td>80</td><td>Square</td><td>1.33</td><td>-</td><td>-</td><td>-</td><td>-</td><td>ref.22</td></tr>
<tr><td rowspan="2">60</td><td rowspan="2">110 - 140</td><td rowspan="2">50 - 80</td><td>80</td><td>Square</td><td rowspan="2">1.0-1.6</td><td rowspan="2">0.15 - 0.45</td><td rowspan="2">150 -300</td><td rowspan="2">350 -600</td><td>0.06</td><td rowspan="2">ref.23</td></tr>
<tr><td>80</td><td>Hexagonal</td><td>0.15</td></tr>
<tr><td>50</td><td>120</td><td>70</td><td>60</td><td>Hexagonal</td><td>0.86</td><td>-</td><td>-</td><td>-</td><td>-</td><td>ref.24</td></tr>
<tr><td>40</td><td>100</td><td>60</td><td>51 - 70</td><td>Square</td><td>0.85 - 1.15</td><td>0.21±0.03</td><td>84.8 ± 18.4</td><td>455.6 ± 45.3</td><td>0.13 ± 0.05</td><td>NemaFlex</td></tr>
</table>

Notes and references

1. N. Otsu, *IEEE Transactions on Systems, Man, and Cybernetics*, 1979, **9**, 62-66.
2. R. M. Haralick and G. S. Linda, *Computer and Robot Vision*, Addison-Wesley, Boston, 1992.
3. D. H. Ballard, *Pattern Recognition*, 1981, **13**, pp. 111-122.
4. S. Timoshenko and J. M. Gere, *Mechanics of Materials*, Van Nostrand Reinhold Co., New York, New York, 1972.
5. P. Du, I. Lin, H. Lu and X. Zhang, *Journal of Micromechanics and Microengineering*, 2010, **20**.
6. Y. Xiang and D. LaVan, *Applied Physics Letters*, 2007, **90**.
7. I. Lin, Y. Liao, Y. Liu, K. Ou, K. Chen and X. Zhang, *Applied Physics Letters*, 2008, **93**.
8. S. Khare, A. Awasthi, V. Venkataraman and S. Koushika, *Biomicrofluidics*, 2015, **9**, 014111.
9. F. Schneider, T. Fellner, J. Wilde and U. Wallrabe, *Journal of Micromechanics and Microengineering*, 2008, **18**.
10. P. Du, X. Zheng, I. Lin and X. Zhang, *Applied Physics Letters*, 2011, **99**.
11. A. Ghanbari, V. Nock, S. Johari, R. Blaikie, X. Chen and W. Wang, *Journal of Micromechanics and Microengineering*, 2012, **22**, 095009.
12. X. Liu, Y. Sun, W. Wang and B. Lansdorp, *Journal of Micromechanics and Microengineering*, 2007, **17**, 1281-1288.
13. S. Johari, V. Nock, M. Alkaisi and W. Wang, *Lab on a Chip*, 2013, **13**, 1699-1707.
14. D. Albrecht and C. Bargmann, *Nature Methods*, 2011, **8**, 599–605.
15. X. Shen, J. Sznitman, P. Krajacic, T. Lamitina and P. Arratia, *Biophysical Journal*, 2012, **102**, 2772-2781.